ACS Macro Letters

Letter

Cite This: ACS Macro Lett. 2019, 8, 1635−1641

pubs.acs.org/macroletters

# Deformation of Chemically Heterogeneous Interfacial Layers of Polymer Nanocomposites

Siyang Yang and Pinar Akcora*

Department of Chemical Engineering & Materials Science, Stevens Institute of Technology, Hoboken, New Jersey 07030, United States

Supporting Information

**ABSTRACT:** Dynamics of entangled interfacial polymer layers around nanoparticles determine the linear rheological properties of polymer nanocomposites. In this study, the nonlinear elastic properties of nanocomposites are examined under large-amplitude oscillatory shear (LAOS) flow to reveal the effect of interfacial chemical heterogeneity on the deformation mechanism of polymer-grafted and polymer-adsorbed nanoparticle composites. Adsorbed-poly(methyl methacrylate) (PMMA) layers presented stronger interfacial stiffening and reinforcement than PMMA-grafted layers. Chemical heterogeneities of interfacial layers, provided by polymer-adsorbed and low graft density particles, deformed at smaller strains than the poly(ethylene oxide) (PEO) matrix. Interfaces of loosely bound PMMA and PEO exhibited stiffening at low strains due to the enhanced chain mixing and entanglements. These results demonstrate that chemical and dynamic heterogeneities in interfacial layers have significant importance in designing adaptive polymer nanocomposites for large shear deformation.

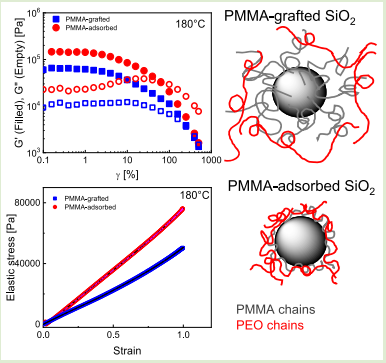




Attractive interactions between particles and polymer chains control not only the good dispersion state of particles in nanocomposites but also the dynamics of polymer chains on particle surfaces.[1−7] Dispersion of fillers, percolation of particles, and bridging between interfacial bound chains are known to control the reinforcement in composites.[8−10] In previous works, the dynamics and structural conformations of adsorbed polymer layers are investigated in composites with chemically identical adsorbed and matrix chains.[11−17] The chemical heterogeneity in interfacial polymer layers offers intriguing dynamic properties that depend on dynamic confinement and coupling phenomena of polymer blends.[18−20]

One unique example of chemical and dynamic heterogeneity was shown for silica nanoparticles adsorbed with a high glass transition temperature polymer poly(methyl methacrylate) (PMMA, $T_g$: 108 °C) and dispersed in a low glass transition temperature polymer, poly(ethylene oxide) (PEO, $T_g$: −60 °C), matrix.[21] Thermal stiffening was achieved with increasing temperature, and this reversible behavior was shown to be due to the fast dynamics of PEO chains in the glassy part of the interfacial chains measured in neutron spin−echo spectroscopy experiments.[22] Spin−echo results revealed that PEO chains can disentangle within the dynamically frozen interfacial layer. Consequently, tube dilation occurs at the interface when bound polymer (PMMA) is glassy.[22] Above the glass transition temperature of PMMA, adsorbed PMMA can easily dynamically couple with PEO matrix chains. This dynamic coupling slows the dynamics of PEO and hence stiffens the matrix polymer at temperatures higher than $T_g$'s of both polymers. The interface layer is thus described to be *dynamic* since both polymers in the interfacial layer have temperature-dependent dynamic heterogeneities.

Nanocomposites with the tightly bound and rigid poly(2-vinylpyridine) (P2VP, $C_\infty$: 10) interface layer, on the other hand, softens with increasing temperature.[23] This interface will be referred to as a weak interface as opposed to the strong interface with the PMMA chains in the rest of the paper. First, we present the LAOS results of the PMMA- and P2VP-adsorbed particle nanocomposites to assess how the different conformation of adsorbed chains that is controlled with particle−polymer interactions can be distorted. Second, nonlinear behavior of PMMA-grafted, PMMA-adsorbed, and bare nanoparticles dispersed in the PEO matrix is analyzed in Fourier transform rheology (FTR) to understand the interfacial dynamic contribution to strain stiffening. Next, we discuss the extent of entanglements in the interfacial layers of grafted nanoparticles versus adsorbed particles with the large-amplitude oscillatory shear flow results. Table 1 shows the characteristics of our samples. Adsorption and grafting protocols, thermal gravimetric analysis (TGA) profiles (Figure S1), and composite preparation are presented in the Supporting Information.

The linear viscoelastic behavior of 50 nm PMMA- and P2VP-adsorbed composites at 85 °C (below $T_g$ of PMMA) and 180 °C (above $T_g$ of PMMA) with 40 wt % particle loading is presented in Figure S2. At 180 °C, a slight upturn of the modulus in the low-frequency regime is seen for the PMMA-adsorbed composite at 40 wt %. The enhancement of storage modulus (also seen for 20 wt %[24]) cannot be explained

**Received:** October 21, 2019
**Accepted:** November 26, 2019




DOI: 10.1021/acsmacrolett.9b00821
ACS Macro Lett. 2019, 8, 1635−1641

**Table 1. Particle Diameter; Grafting Density of Polymer-Coated $SiO_2$ Nanoparticles through Adsorption and Chemical Grafting; and Particle Loading of PEO Nanocomposites Studied in Linear and Nonlinear Tests**

| $SiO_2$ diameter (nm) | polymer-modified particles | adsorbed/grafted polymer MW (kDa) | bound or grafting density (chains/nm$^2$) | bound or grafting density (chains/particle) | particle loading (wt %) |
|---|---|---|---|---|---|
| 50 | bare | - | - | - | 40 |
| 50 | PMMA-ads | 118 | 0.005 | 41 | 40 |
| 50 | P2VP-ads | 40 | 0.016 | 140 | 40 |
| 20 | bare | - | - | - | 30 |
| 20 | PMMA-ads | 188 | 0.001 | 2 | 30 |
| 20 | PMMA-gr | 203 | 0.007 | 9 | 30 |
| 20 | PMMA-gr | 261 | 0.016 | 20 | 30 |
| 20 | PMMA-gr | 230 | 0.028 | 36 | 30 |

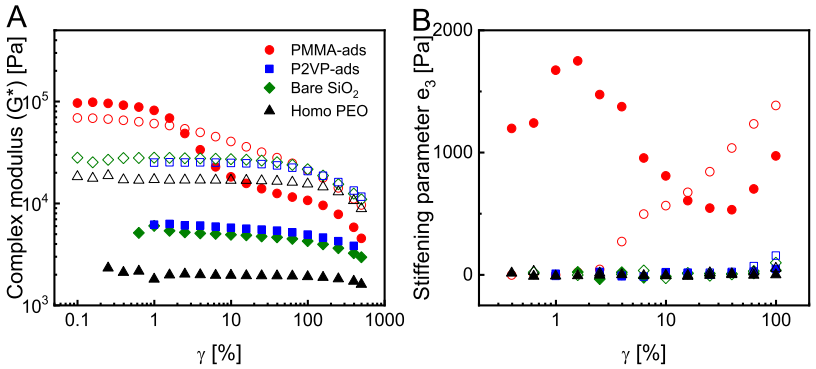


**Figure 1.** (A) Strain dependency of the complex modulus ($G^*$) and (B) the third-order elastic Chebyshev coefficients ($e_3$) for 50 nm 118 kDa PMMA-adsorbed, 40 kDa P2VP-adsorbed $SiO_2$, and bare $SiO_2$ in 100 kDa PEO composites at 85 and 180 °C with 40 wt % loading. Filled symbols represent the complex moduli measured at 180 °C, and open symbols represent measurements at 85 °C in panels A and B.

by the particle percolation or by dispersion states which are similar in PMMA- and P2VP-adsorbed particles for the corresponding loadings. Instead, we attribute this behavior to the interfacial chain relaxations. This is consistent with our previous findings[2,3] which showed that the mobile PMMA chains can dynamically couple with the PEO matrix at temperatures above the $T_g$ of adsorbed (PMMA) chains, hence highly entangled chains yield stronger interfacial resistance to deformation. Overall, the low frequency elastic modulus data imply a stronger interfacial effect of the more mobile PMMA-adsorbed sample than the more rigid P2VP-adsorbed sample. The normalized elastic moduli of composites at the deformed state with respect to their initial states (Figure S3) suggests this reinforcement was enhanced after LAOS.[24] Since particle dispersion did not change after applying LAOS (as seen in SEM in Figures S4 and S5 before and after deformation, respectively), the measured reinforcement was associated with the interfacial entanglement states as also proposed in our earlier works on PMMA composites.[16,25] SAXS data of composites before deformation are also shown in Figure S4, revealing the good dispersion of bare and adsorbed particles in PEO.

We applied sinusoidal strains $\gamma(t) = \gamma_0 \sin(\omega t)$ from $\gamma_0$ = 0.1% to $\gamma_0$ = 300% at a fixed frequency of $\omega$ = 5 rad/s. The strain sweep data and the critical strain where the Payne effect is seen for the PMMA- and P2VP-adsorbed composites are discussed in Figure 1A. Two nonlinear steps at strains of 1% and 100% are identified at 180 °C in the PMMA-adsorbed composite, whereas one nonlinear step around 1% strain is measured at 85 °C (Figure 1A, shown with open symbols). The unexpected decrease in modulus around low strain (1%) of the PMMA-adsorbed particles is attributed to the deformation of the interfacial layer where PMMA and PEO dynamically couple at 180 °C. The modulus drop at large strain (around 100%) is a result of disentanglement and alignment of PEO matrix chains with shear flow. At 85 °C, the interfacial layer with the glassy PMMA and melt PEO chains is not well entangled, hence the absence of dynamic coupling leads to lower $G^*$ of the PMMA-adsorbed composite. The steady decrease of $G^*$ at 85 °C is similar to that seen in bare composites but with much larger $G^*$, indicating the effect of dynamic heterogeneities in the PMMA-adsorbed composite. Tightly bound P2VP-adsorbed composites goes through similar nonlinear behavior as bare nanocomposites. This suggests that the interfacial layer entanglement and conformations of chains do not change in the weak interfaces under large shear flow. These results are supported by a stiffening parameter, $e_3$, obtained from the FTR data analysis which is described below.

FTR expresses the total nonlinear stress response to sinusoidal excitation as a sum of infinite set of sine and cosine functions with odd integer multiples of the fundamental frequency $\sigma(t; \omega, \gamma_0) = \gamma_0 \sum_{n:\text{odd}} G'(\omega, \gamma_0)\sin(n\omega t) + G''(\omega, \gamma_0)\cos(n\omega t)$ with $G'_n$ being the modulus at the $n$th harmonic.[26] The relative intensity of the higher harmonics with respect to fundamental frequency, $I_n/I_1$, has been used to relate the nonlinearities to the materials' properties.[27−30] Rogers et al.[31,32] analyzed the nonlinear stress response and interpreted each harmonics as a sequence of physical processes in colloidal glasses such as linear stress increase, yielding, flow, and reformation. The measured total stress is decomposed into two constructions as known as elastic $\sigma_e$ and viscous $\sigma_v$ stresses using the MITLaos


DOI: 10.1021/acsmacrolett.9b00821
ACS Macro Lett. 2019, 8, 1635−1641

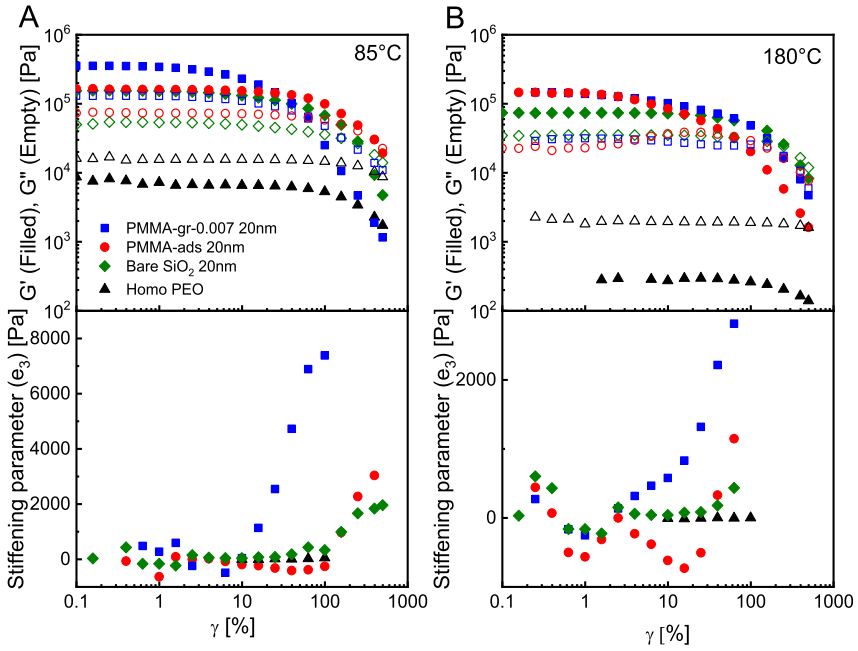


**Figure 2.** Storage and loss moduli and third-order elastic Chebyshev coefficients ($e_3$) of strain sweep results for 20 nm 188 kDa PMMA-adsorbed, 203 kDa PMMA-grafted $SiO_2$, and bare $SiO_2$ in PEO (100 kDa) composites and the PEO homopolymer at (A) 85 °C and (B) 180 °C for 30 wt % loading.

software.[33,30] The orthonormal decomposition of the elastic and viscous stresses is described with the Chebyshev polynomials of the first kind as $\sigma_e(x, \omega, \gamma) = \gamma_0 \sum_{n:\text{odd}} e_n(\omega, \gamma_0) T_n(x)$, where $T_n$ is the $n$th order polynomial; $e_n$ is the corresponding elastic coefficient; and $x = \gamma/\gamma_0$.[34,35] $e_1$ represents the average stored energy per unit volume within an oscillation cycle and equals $G_1'$, and $e_3$ represents the deviations from average response at large strains. The positive $e_3$ represents strain stiffening, and negative $e_3$ indicates softening within an oscillation cycle. Here, we used Chebyshev polynomial analysis to obtain $e_1$ and $e_3$. Figure 1B shows the elastic Chebyshev coefficients ($e_3$) in the strain sweep tests. At 85 °C, the $e_3$ values of P2VP-adsorbed and bare composites and PEO homopolymer are at near-zero values up to 100% strain, meaning a linear viscoelastic behavior. The PMMA-adsorbed composite shows strain stiffening response with positive $e_3$ values when the PMMA layer is glassy. This stiffening at 85 °C simply arises from the stretching of matrix chains. In the molten state (at 180 °C), the adsorbed composite shows stiffening at small strains ($\gamma \sim 1\%$) as a result of rearrangements in the strong interfacial layer. The strain stiffening is not seen in the P2VP-adsorbed composite. Dense conformation of P2VP chains presumably hinders the diffusion of PEO chains, creating lower entanglement density in interfacial layers.

The interfacial chain confinement becomes more effective for the small nanoparticles used in adsorbed samples which then leads to the higher linear elastic moduli at both temperatures (Figure S6) despite the lower particle loading at 30 wt % in these composites. The nonlinear behavior of the more confined system (with 20 nm particles) shows non-linearity at 100% strain, and its $G''$ increases at 10% strain, indicating some energy dissipation when PMMA chains disentangle or desorb from particles during deformation, unlike the two transitions seen with 50 nm particles at 180 °C (Figure S7).

Next, we will discuss the interfaces created with grafted and adsorbed particles of the same diameter (20 nm). The linear viscoelastic behavior of grafted, adsorbed, and bare composites is presented in Figure S8. At 85 °C, the low-frequency dependence of viscoelastic moduli of the grafted sample suggests stronger interparticle interactions, clearly indicating deviation from an entangled melt dynamics. In this confined limit, bridging of grafted chains at 85 °C creates stronger network than the adsorbed particles. At 180 °C, however, adsorbed particles behave unusually more reinforced than the grafted particles due to the stronger dynamic coupling between mobile PMMA-adsorbed loops and the matrix chains. The mixing and entanglement states of PEO in the interfacial layer of grafted particles are not as good as in the adsorbed samples. This mixing factor informs the dispersion states of particles, which is verified by SAXS experiments. SAXS data modeled with the one-level Unified model gave mass fractal dimension of 3.8 for particles with radius of 10.7 and 13.3 nm for bare and PMMA-adsorbed $SiO_2$, respectively, close to the actual 20 nm particle diameter (Figure S9 and Table S2). Particles with low grafting density and long grafted chains form connected structures as a result of the bridging between grafted chains. We found fractal dimension to be 2.8 for the grafted sample indicating the surface fractal characteristics for the grafted aggregates.

The nonlinear data of bare, grafted, and adsorbed particles at 85 and 180 °C are presented in Figure 2. At 85 °C, strain-dependent $G'$ values of adsorbed and bare composites overlap. The nonlinear region for grafted particles starts at smaller strain (6%) than adsorbed and bare composites (~20%) at 85 °C (Figure 2A), which is explained with the low penetration of PEO with grafted chains as also suggested with the linear data. At 180 °C, the nonlinearity starts at 8% strain for both grafted and adsorbed composites (Figure 2B). It is difficult to interpret the strain data without comparing the strain stiffening coefficient ($e_3$). As shown in Figures 2A,B, the $e_3$ of the



DOI: 10.1021/acsmacrolett.9b00821
ACS Macro Lett. 2019, 8, 1635−1641

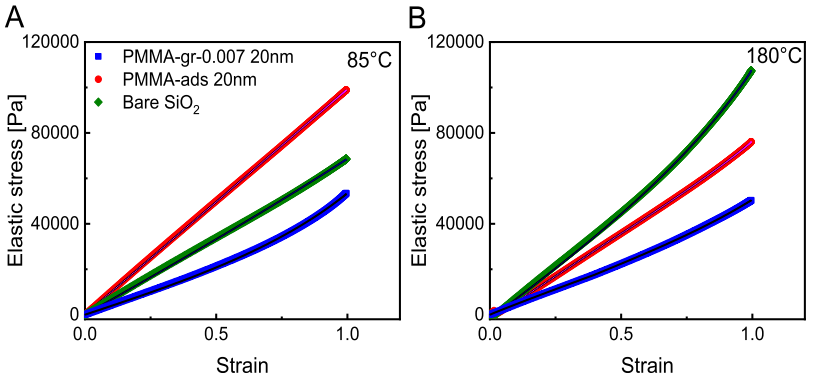


**Figure 3.** Stress−strain curves of 20 nm 188 kDa PMMA-adsorbed, 203 kDa PMMA-grafted (0.007 chains/nm$^2$), and bare particles in the 100 kDa PEO matrix at (A) 85 °C and (B) 180 °C. Black lines represent the polymer network model fits.

grafted composite increases between 2% and 10% strain and reaches to a finite chain extension at 100% strain at 85 and 180 °C as a result of the stretching and alignment of matrix chains at larger strains. At 180 °C and intermediate strains, the bridging between grafted chains cannot break but slightly rearranges and enhances entanglements between the mobile PMMA and PEO matrix chains. Contrary to this behavior, the adsorbed composite softens at both temperatures. Loop conformation of adsorbed PMMA can entrap and create additional topological constraints for PEO at interfacial layers, hence the large deformation would break this interaction by desorbing or disentangling the PMMA chains, leading to the strain softening and energy dissipation. The bare composite presents lower softening behavior than the PMMA-adsorbed composite, suggesting that the deformability of chemically heterogeneous layers is easier at large strains.

These results provide a new insight into the thermal stiffening behavior of our composites. The denser entanglements and mixing at the interface layer occur between PMMA-adsorbed loops and PEO matrix chains; hence, stiffening at temperatures above $T_g$ of PMMA enhances with LAOS. As chains relax after deformation, the desorbed or disentangled PMMA loops are rearranged to form a denser interfacial layer with better mixing, leading to a reinforcement effect at high temperature. The normalized elastic moduli of PMMA-adsorbed composites at the deformed state with respect to their initial states in Figure S10 confirm the enhanced reinforcement after LAOS.

Total elastic stress−strain data of all the samples are shown in Figure 3, and a nonlinear mechanistic model developed for polymer chains and networks under deformation by Dobrynin et al.[36] was applied to our LAOS data. The stress response of the polymer coil was expressed as $\sigma = \frac{G_{pol}\gamma}{3}\left[1 + 2\left(1 - \frac{\beta I_1(\gamma)}{3}\right)^{-2}\right]$ where $G_{pol}$ is the shear modulus of the polymer. $I_1(\gamma) = (\gamma^2 + 3)$ is the first invariant for the shear deformation, and $\beta$ is the chain elongation ratio which is defined as the mean square of the end-to-end distance of an unperturbed chain to the square of the end-to-end distance of the fully extended strand, $\beta = \langle R_{in}^2\rangle/R_{max}^2$. However, at a temperature above $T_g$ of adsorbed chains, the adsorbed and grafted PMMA chains get mobile and entangle well with PEO matrix chains. We added a nonlinear elastic term, $G_{inter}\gamma^n$, for the small-amplitude regime (prior to the matrix chain stretching or alignment regime, 40% strain for the adsorbed sample and 20% for the grafted sample in Figure 3), where $G_{inter}$ is the shear modulus of the interface and $n$ is the strain softening parameter. The total stress for adsorbed and grafted samples at 180 °C is, therefore, expressed as

$$\sigma = G_{inter}\gamma^n, \quad \gamma < \gamma_y$$

$$\sigma = \frac{G_{pol}(\gamma - \gamma_y)}{3}\left[1 + 2\left(1 - \frac{\beta I_1(\gamma - \gamma_y)}{3}\right)^{-2}\right] + G_{inter}\gamma_y^n, \quad \gamma_y < \gamma < \gamma_0$$

As shown in Table 2, the elongation parameters of adsorbed and bare samples are the same at 85 °C (0.08), suggesting the glassy PMMA-adsorbed chains do not affect the stretching of PEO matrix chains. The interfacial layer of the adsorbed sample (shown with red data) and its better dispersion state clearly contribute to the strengthening of the adsorbed composite (Figure 3A). When the PMMA chains are mobile at 180 °C, the $\beta$ (chain elongation ratio) value of the adsorbed and grafted samples increases to 0.26 and 0.49, respectively, whereas $\beta$ of the bare sample stays the same (0.08) as it is at 85 °C. The mobile PMMA chains entangle with PEO matrix chains, and the stronger interfacial interaction limits the stretchability of PEO matrix chains. The large elongation of PEO matrix chains in the bare sample is the reason for the highest elastic stress at 180 °C (Figure 3B). The higher interface modulus $G_{inter}$ of the adsorbed sample indicates a stronger interfacial interaction of PMMA-adsorbed loops and PEO chains. The softening parameter ($n$) is found to be 1, higher than that of the grafted sample, suggesting the interfacial layer deformability. $G_{pol}$ values of all the samples are consistent with the moduli values at 100% strain. In

**Table 2. Shear Modulus of Bulk Polymer ($G_{pol}$), Elongation Ratio ($\beta$), Shear Modulus of Polymer Interface ($G_{inter}$), and Strain-Softening Parameter of the Interface ($n$) at 85 °C and 180 °C Are Found from the Polymer Network Model Fittings to the Stress−Strain Data of Bare, PMMA-Adsorbed, and PMMA-Grafted Composites**

| | $G_{pol}$ (Pa) | $\beta$ | $G_{pol}$ (Pa) | $\beta$ | $G_{inter}$ (Pa) | $n$ |
|---|---|---|---|---|---|---|
| | 85 °C | 85 °C | 180 °C | 180 °C | 180 °C | 180 °C |
| bare | 58635 | 0.08 | 89853 | 0.08 | | |
| adsorbed | 87660 | 0.08 | 47471 | 0.26 | 75222 | 1 |
| grafted | 20483 | 0.34 | 5900 | 0.49 | 19619 | 0.86 |



DOI: 10.1021/acsmacrolett.9b00821
ACS Macro Lett. 2019, 8, 1635−1641

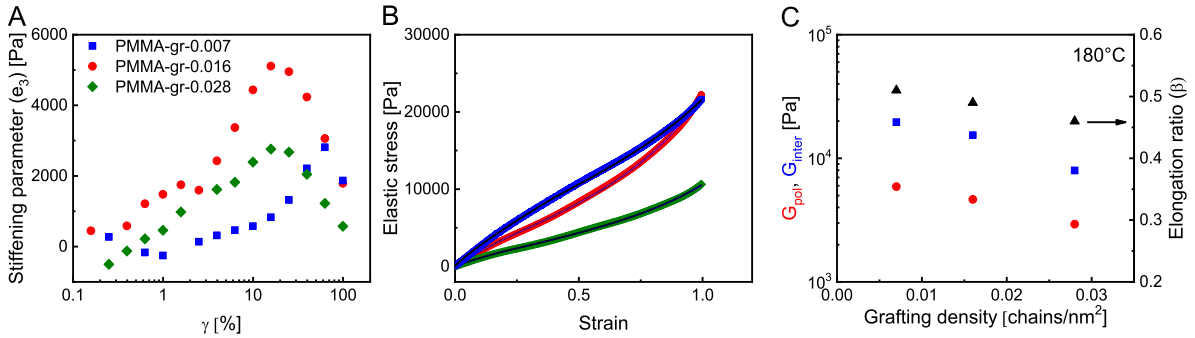


**Figure 4.** (A) Third-order elastic Chebyshev coefficients ($e_3$) for 20 nm PMMA-grafted $SiO_2$ with different grafting densities (0.007, 0.016, and 0.028 chains/nm$^2$) in 100 kDa PEO composites at 180 °C at 30 wt % loading. (B) Elastic stress−strain curves of grafted composites at 180 °C. Black lines are the model fits. (C) $G_{pol}$, $G_{inter}$, and $\beta$ values deduced from elastic stress fittings with two components versus grafting density at 180 °C of PEO composites.

summary, using polymer blends with $T_g$ disparity, it is possible to differentiate the interfacial layer contribution to strain stiffening in composites. These results suggest that chemical heterogeneity in the interfacial layer enhances the nonlinear mechanical properties of the composite.

Another important property that influences the mixing of two different polymers in the interfacial layer is the grafting density. The linear frequency data show that the elastic modulus increases with decreasing grafting density (Figure S11A) at the low frequency range. At 180 °C, the low grafting density sample (0.007 chains/nm$^2$) behaves like a network as observed in the frequency-independent storage modulus (Figure S11B), whereas the higher grafting density samples (0.016 and 0.028 chains/nm$^2$) show the network behavior only at the low frequency range, suggesting the entanglement density is higher with the low grafting density. SAXS data of the three grafted composites (in Figure S12) were fitted with the two-level Unified model, and the fitting parameters are shown in Table S2. The level one fitting shows that the radii are 35.8, 38.6, and 38.1 nm for grafted $SiO_2$ samples in the order of increasing grafting density, suggesting that 2−3 particle size clusters exist. The fractal dimension increases from 2.8 to 3.1 with grafting density. The lower fractal dimension indicates the low grafting density sample has stronger interparticle interactions that form connected structures as a result of the bridging between grafted chains.

The FTR rheology analysis on three grafting systems shows high stiffening effect at large strains (Figure 4A). For intermediate and high graft density, stiffening parameter ($e_3$) presents a maximum at 10% strain, whereas the low graft density sample shows stiffening up to 100% strain. This indicates the interfacial chain entanglements should be denser in the low grafting density sample, and interfacial chains mix and deform rather than disentangling under large shear. This effect is represented in elastic stress−strain curves (Figure 4B) and in the moduli values for the interface layer deduced from the network model (Figure 4C). The total elastic stress−strain data were fitted with the polymer network model with the interface layer contribution (Figure 4B), and the fitting parameters were displayed in Table S3. Both $G_{pol}$ and $G_{inter}$ values and $\beta$ decrease with increasing grafting density, indicating that the interaction between grafted PMMA and PEO matrix chains was getting weaker (Figure 4C). Linear and nonlinear rheology results both suggest that the better interfacial mixing and entanglement exist in low grafting density PMMA and the PEO interfacial layer.

In conclusion, for the adsorbed composite (50 nm silica particles), better entanglement and dynamic coupling of chains at 180 °C lead to stretching of interfacial chains at low strain (1%) and to the disentangling and stretching of matrix chains at large strains. This deformation of the interfacial layer is compared with the composite where particles were adsorbed with a densely packed P2VP layer. The weak interface of P2VP−PEO of this composite cannot be deformed as shown with the low strain stiffening parameter at low-to-medium strains. The results simply verify that interfacial deformation occurs at low strains with the mobile adsorbed layer. By analyzing the elastic stresses below and above the glass-transition temperature of PMMA, we found that more energy is needed to deform the interfacial chains of the adsorbed composites at 180 °C. The stronger interfacial mixing, entanglement, and reinforcement were observed with low grafting density. In summary, the interfacial layer of adsorbed and matrix chains with neutral polymer−polymer interactions (as in PMMA−PEO) can deform. Knowing the deformability of interfacial layers allows us to choose dynamically asymmetric blends for mechanically adaptive and stiffening composites that can perform for large shear and high-temperature applications.

## ■ ASSOCIATED CONTENT

### Supporting Information

The Supporting Information is available free of charge at https://pubs.acs.org/doi/10.1021/acsmacrolett.9b00821.

Materials; synthesis of grafted nanoparticles; composite preparation; grafting density calculation; rheological and structural characterization details. Supporting figures on TGA data of PMMA-grafted and PMMA- and P2VP-adsorbed particles; linear viscoelastic data of PMMA-adsorbed, PMMA-grafted, P2VP-adsorbed, and bare particles in PEO composites; normalized elastic moduli of PMMA-adsorbed and P2VP-adsorbed particles at two temperatures; SAXS and SEM data of the 50 nm adsorbed composites; SEM images of bare and PMMA-adsorbed composites after LAOS application; comparison of frequency sweep and strain sweep data of different particle sizes; linear data of bare, PMMA-grafted, and PMMA-adsorbed composites; SAXS profiles of adsorbed, grafted, and bare composites; linear data of grafted particles at varying graft densities; and SAXS profiles of particles at different graft densities in PEO composites (PDF)



DOI: 10.1021/acsmacrolett.9b00821
ACS Macro Lett. 2019, 8, 1635−1641

## AUTHOR INFORMATION


### Corresponding Author

*Email: pakcora@stevens.edu.

### ORCID

Pinar Akcora: 0000-0001-7853-7201


### Notes

The authors declare no competing financial interest.

## ACKNOWLEDGMENTS

This material is based upon work supported by the National Science Foundation CMMI MEP program under Grant No. 1825250. We thank Prof. Sanat Kumar and graduate student Andrew Jimenez from Columbia University for the SAXS measurements.

## REFERENCES


(1) Cheng, S.; Bocharova, V.; Belianinov, A.; Xiong, S.; Kisliuk, A.; Somnath, S.; Holt, A. P.; Ovchinnikova, O. S.; Jesse, S.; Martin, H.; Etampawala, T.; Dadmun, M.; Sokolov, A. P. Unraveling the mechanism of nanoscale mechanical reinforcement in glassy polymer nanocomposites. *Nano Lett.* **2016**, *16* (6), 3630−3637.

(2) Lin, C. C.; Gam, S.; Meth, J. S.; Clarke, N.; Winey, K. I.; Composto, R. J. Do attractive polymer-nanoparticle interactions retard polymer diffusion in nanocomposites? *Macromolecules* **2013**, *46* (11), 4502−4509.

(3) Merabia, S.; Sotta, P.; Long, D. R. A microscopic model for the reinforcement and the nonlinear behavior of filled elastomers and thermoplastic elastomers (Payne and Mullins Effects). *Macromolecules* **2008**, *41* (21), 8252−8266.

(4) Moll, J.; Kumar, S. K. Glass transitions in highly attractive highly filled polymer nanocomposites. *Macromolecules* **2012**, *45* (2), 1131−1135.

(5) Zhu, A. J.; Sternstein, S. S. Nonlinear viscoelasticity of nanofilled polymers: Interfaces, chain statistics and properties recovery kinetics. *Compos. Sci. Technol.* **2003**, *63* (8), 1113−1126.

(6) Bogoslovov, R. B.; Roland, C. M.; Ellis, A. R.; Randall, A. M.; Robertson, C. G. Effect of silica nanoparticles on the local segmental dynamics in poly(vinyl acetate). *Macromolecules* **2008**, *41* (4), 1289−1296.

(7) Krutyeva, M.; Wischnewski, A.; Monkenbusch, M.; Willner, L.; Maiz, J.; Mijangos, C.; Arbe, A.; Colmenero, J.; Radulescu, A.; Holderer, O.; Ohl, M.; Richter, D. Effect of nanoconfinement on polymer dynamics: Surface layers and interphases. *Phys. Rev. Lett.* **2013**, *110* (10), 119901.

(8) Jouault, N.; Vallat, P.; Dalmas, F.; Said, S.; Jestin, J.; Boue, F. Well-dispersed fractal aggregates as filler in polymer-silica nanocomposites: Long-range effects in rheology. *Macromolecules* **2009**, *42* (6), 2031−2040.

(9) Zhao, D.; Ge, S.; Senses, E.; Akcora, P.; Jestin, J.; Kumar, S. K. Role of Filler Shape and Connectivity on the Viscoelastic Behavior in Polymer Nanocomposites. *Macromolecules* **2015**, *48* (15), 5433−5438.

(10) Akcora, P.; Kumar, S. K.; Moll, J.; Lewis, S.; Schadler, L. S.; Li, Y.; Benicewicz, B. C.; Sandy, A.; Narayanan, S.; Ilavsky, J.; Thiyagarajan, P.; Colby, R. H.; Douglas, J. F. "Gel-like" mechanical reinforcement in polymer nanocomposite melts. *Macromolecules* **2010**, *43* (2), 1003−1010.

(11) Papon, A.; Montes, H.; Lequeux, F.; Oberdisse, J.; Saalwächter, K.; Guy, L. Solid particles in an elastomer matrix: Impact of colloid dispersion and polymer mobility modification on the mechanical properties. *Soft Matter* **2012**, *8* (15), 4090−4096.

(12) Cheng, S.; Xie, S. J.; Carrillo, J. M. Y.; Carroll, B.; Martin, H.; Cao, P. F.; Dadmun, M. D.; Sumpter, B. G.; Novikov, V. N.; Schweizer, K. S.; Sokolov, A. P. Big Effect of Small Nanoparticles: A Shift in Paradigm for Polymer Nanocomposites. *ACS Nano* **2017**, *11* (1), 752−759.

(13) Carrillo, J. M. Y.; Cheng, S.; Kumar, R.; Goswami, M.; Sokolov, A. P.; Sumpter, B. G. Untangling the Effects of Chain Rigidity on the Structure and Dynamics of Strongly Adsorbed Polymer Melts. *Macromolecules* **2015**, *48* (12), 4207−4219.

(14) Senses, E.; Tyagi, M.; Natarajan, B.; Narayanan, S.; Faraone, A. Chain dynamics and nanoparticle motion in attractive polymer nanocomposites subjected to large deformations. *Soft Matter* **2017**, *13* (43), 7922−7929.

(15) Senses, E.; Ansar, S. M.; Kitchens, C. L.; Mao, Y.; Narayanan, S.; Natarajan, B.; Faraone, A. Small Particle Driven Chain Disentanglements in Polymer Nanocomposites. *Phys. Rev. Lett.* **2017**, *118* (14), 147801.

(16) Senses, E.; Akcora, P. An interface-driven stiffening mechanism in polymer nanocomposites. *Macromolecules* **2013**, *46* (5), 1868−1874.

(17) Akcora, P.; Kumar, S. K.; García Sakai, V.; Li, Y.; Benicewicz, B. C.; Schadler, L. S. Segmental dynamics in PMMA-grafted nanoparticle composites. *Macromolecules* **2010**, *43* (19), 8275−8281.

(18) Haley, J. C.; Lodge, T. P. Dynamics of a poly(ethylene oxide) tracer in a poly(methyl methacrylate) matrix: Remarkable decoupling of local and global motions. *J. Chem. Phys.* **2005**, *122* (23), 234914.

(19) Tyagi, M.; Arbe, A.; Alegría, A.; Colmenero, J.; Frick, B. Dynamic confinement effects in polymer blends. A quasielastic neutron scattering study of the slow component in the blend poly(vinyl acetate)/poly(ethylene oxide). *Macromolecules* **2007**, *40* (13), 4568−4577.

(20) Tyagi, M.; Arbe, A.; Colmenero, J.; Frick, B.; Stewart, J. R. Dynamic confinement effects in polymer blends. A quasielastic neutron scattering study of the dynamics of poly(ethylene oxide) in a blend with poly(vinyl acetate). *Macromolecules* **2006**, *39* (8), 3007−3018.

(21) Senses, E.; Isherwood, A.; Akcora, P. Reversible thermal stiffening in polymer nanocomposites. *ACS Appl. Mater. Interfaces* **2015**, *7* (27), 14682−14689.

(22) Senses, E.; Faraone, A.; Akcora, P. Microscopic Chain Motion in Polymer Nanocomposites with Dynamically Asymmetric Interphases. *Sci. Rep.* **2016**, *6*, 29326.

(23) Yang, S.; Liu, S.; Narayanan, S.; Zhang, C.; Akcora, P. Chemical heterogeneity in interfacial layers of polymer nanocomposites. *Soft Matter* **2018**, *14* (23), 4784−4791.

(24) Yang, S.; Hassan, M.; Akcora, P. Role of adsorbed chain rigidity in reinforcement of polymer nanocomposites. *J. Polym. Sci., Part B: Polym. Phys.* **2019**, *57* (1), 9−14.

(25) Senses, E.; Jiao, Y.; Akcora, P. Modulating interfacial attraction of polymer-grafted nanoparticles in melts under shear. *Soft Matter* **2014**, *10* (25), 4464−4470.

(26) Giacomin, A. J.; Dealy, J. M., Large-amplitude oscillatory shear. In *Techniques in rheological measurement*; Springer: 1993; pp 99−121.

(27) Hyun, K.; Wilhelm, M. Establishing a new mechanical nonlinear coefficient Q from FT-rheology: First investigation of entangled linear and comb polymer model systems. *Macromolecules* **2009**, *42* (1), 411−422.

(28) Hyun, K.; Ahn, K. H.; Lee, S. J.; Sugimoto, M.; Koyama, K. Degree of branching of polypropylene measured from Fourier-transform rheology. *Rheol. Acta* **2006**, *46* (1), 123−129.

(29) Reinheimer, K.; Grosso, M.; Wilhelm, M. Fourier Transform Rheology as a universal non-linear mechanical characterization of droplet size and interfacial tension of dilute monodisperse emulsions. *J. Colloid Interface Sci.* **2011**, *360* (2), 818−825.

(30) Reinheimer, K.; Grosso, M.; Hetzel, F.; Kübel, J.; Wilhelm, M. Fourier Transform Rheology as an innovative morphological characterization technique for the emulsion volume average radius and its distribution. *J. Colloid Interface Sci.* **2012**, *380* (1), 201−212.

(31) Rogers, S. A.; Erwin, B. M.; Vlassopoulos, D.; Cloitre, M. A sequence of physical processes determined and quantified in LAOS: Application to a yield stress fluid. *J. Rheol.* **2011**, *55* (2), 435−458.

(32) Rogers, S.; Kohlbrecher, J.; Lettinga, M. The molecular origin of stress generation in worm-like micelles, using a rheo-SANS LAOS approach. *Soft Matter* **2012**, *8* (30), 7831−7839.




DOI: 10.1021/acsmacrolett.9b00821
*ACS Macro Lett.* 2019, 8, 1635−1641

(33) Cho, K. S.; Hyun, K.; Ahn, K. H.; Lee, S. J. A geometrical interpretation of large amplitude oscillatory shear response. *J. Rheol.* **2005**, *49*, 747−758.
(34) Ewoldt, R. H.; Hosoi, A.; McKinley, G. H. New measures for characterizing nonlinear viscoelasticity in large amplitude oscillatory shear. *J. Rheol.* **2008**, *52*, 1427−1458.
(35) Cho, K. S., Large amplitude oscillatory shear. In *Viscoelasticity of Polymers*; Springer: Dordrecht, 2016; Vol. *241*, pp 545−599.
(36) Dobrynin, A. V.; Carrillo, J. M. Y. Universality in nonlinear elasticity of biological and polymeric networks and gels. *Macromolecules* **2011**, *44* (1), 140−146.

## NOTE ADDED AFTER ASAP PUBLICATION

This paper was published on the Web on December 2, 2019, with errors on the y-axis labels for Figures 1, 2, and 4. The corrected version was reposted on December 2, 2019.



DOI: 10.1021/acsmacrolett.9b00821
*ACS Macro Lett.* 2019, 8, 1635−1641